

# Connecting Dark Matter Annihilation to the Vertex Functions of Standard Model Fermions

Jason Kumar<sup>1,\*</sup> and Christopher Light<sup>1,†</sup>

<sup>1</sup>*Department of Physics & Astronomy,  
University of Hawaii, Honolulu, HI 96822, USA.*

## Abstract

We consider scenarios in which dark matter is a Majorana fermion which couples to Standard Model fermions through the exchange of charged mediating particles. The matrix elements for various dark matter annihilation processes are then related to one-loop corrections to the fermion-photon vertex, where dark matter and the charged mediators run in the loop. In particular, in the limit where Standard Model fermion helicity mixing is suppressed, the cross section for dark matter annihilation to various final states is related to corrections to the Standard Model fermion charge form factor. These corrections can be extracted in a gauge-invariant manner from collider cross sections. Although current measurements from colliders are not precise enough to provide useful constraints on dark matter annihilation, improved measurements at future experiments, such as the International Linear Collider, could improve these constraints by several orders of magnitude, allowing them to surpass the limits obtainable by direct observation.

arXiv:1612.00773v2 [hep-ph] 26 Apr 2017

---

\* jkumar@hawaii.edu

† lightc@hawaii.edu

## 1. INTRODUCTION

It has long been appreciated that if dark matter (DM) is a Majorana fermion and if the theory respects minimal flavor violation (MFV), then dark matter annihilation to light Standard Model (SM) fermions is  $p$ -wave suppressed in the chiral limit. Nevertheless,  $p$ -wave annihilation can be an important process in the early Universe during the epoch of thermal dark matter freeze-out, when this velocity-suppression is only an  $\mathcal{O}(0.1)$  effect. In the current epoch, when this velocity suppression is large ( $\sim 10^{-6}$ ), indirect detection signals may instead be dominated by other annihilation processes, such as virtual internal bremsstrahlung (IB), or annihilation to photons via a one-loop diagram. In this work, we consider the constraints on these annihilation processes which can arise from associated corrections to the vertex functions of the Standard Model fermions.

If dark matter ( $\chi$ ) annihilates to a charged SM fermion ( $f$ ) through the  $t$ -channel exchange of charged mediating particles, then there is necessarily a one-loop correction to the fermion-photon vertex arising from diagrams where  $\chi$  and the charged mediators run in the loop (see Figure 1). It has previously been shown [1] that the  $s$ -wave dark matter annihilation matrix element is directly correlated with the associated correction to the electric and magnetic dipole moments of the SM fermions. This connection follows from general principles: the annihilation process  $\chi\chi \rightarrow \bar{f}f$  can only proceed from an  $s$ -wave initial state if there is some mixing of SM fermion helicities, and the electromagnetic form factors which contribute to helicity mixing yield the electric and magnetic dipole moments in the limit of small momentum transfer. One might expect that the annihilation matrix elements which do not mix SM fermion Weyl spinors can be similarly correlated with corrections to the electromagnetic form factors which do not mix SM fermion Weyl spinors, and we will see that this is indeed the case. In particular, these annihilation matrix elements can be related to a correction to the helicity-preserving form factor,  $F_1(q^2)$ , in the limit of small momentum transfer.

The first moment of this form factor is sometimes parameterized by a quantity referred to as the charge radius, and one might think of the one-loop correction involving dark matter as providing a correction to the charge radius. However, it is important to be precise about this concept; although the form factor  $F_1(q^2)$  is gauge-invariant in quantum electrodynamics, it is generally not gauge-invariant in a non-Abelian gauge theory (see, for example, [2–4]), such as the Standard Model. Although the isolated diagram which we are interested in, involving dark matter running in the loop, *is* gauge-invariant, there will be other corrections involving only SM particles which are not. But any  $S$ -matrix must be gauge-invariant, and we will find that one can extract constraints on

the correction in which we are interested from collider cross sections.

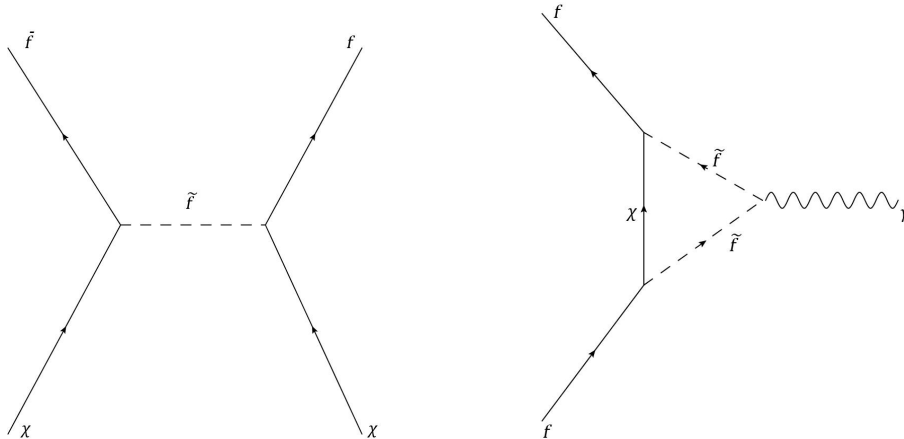


FIG. 1: Feynman diagrams corresponding to the annihilation process  $\chi\chi \rightarrow \bar{f}f$  (left diagram) and to the correction to the fermion-photon vertex (right diagram).

Constraints on corrections to the vertex functions can be inferred from cross section measurements at LEP [5], and future experiments may yield much more precise measurements. We will find that collider constraints can be translated into bounds on the non-helicity-mixing terms of the cross sections for the dark matter annihilation processes  $\chi\chi \rightarrow \bar{f}f, \bar{f}f\gamma, \gamma\gamma$ . But the corrections to Standard Model cross sections at colliders involve all new physics, and can arise both from diagrams involving dark matter, and from new physics unrelated to dark matter. Thus, it is always possible that a large correction arising from loop corrections involving dark matter could be canceled by another large correction arising from unrelated new physics, leaving a smaller total correction to a collider cross section. As a result, the constraints we will find, at a rigorous level, really indicate the extent to which one must fine-tune different corrections in order to retain consistency with the data.

We will see that current bounds from LEP are not precise enough to be useful. But future analyses, particularly using colliders with higher energy and luminosity than LEP, could provide much better measurements of SM fermion vertex functions, potentially improving the resulting constraints on dark matter annihilation processes by several orders of magnitude. In this case, the resulting constraints could not only be relevant for constraining models of dark matter annihilation in the early Universe, but could exceed limits obtainable in the current epoch from direct observation.

The plan of this paper is as follows. In Section 2, we describe the relationship between the SM fermion vertex function correction and the annihilation cross sections for the processes  $\chi\chi \rightarrow$

$\bar{f}f, \bar{f}f\gamma, \gamma\gamma$ . In section 3, we determine the constraints imposed on dark matter annihilation, both in the early Universe and in the present epoch, from current and potential measurements at colliders. We conclude in section 4 with a discussion of our results.

## 2. CONNECTING DARK MATTER ANNIHILATION TO THE FERMION VERTEX CORRECTION

We first consider the scenario in which a Majorana fermion dark matter particle ( $\chi$ ) annihilates to a SM charged fermion/anti-fermion pair ( $\bar{f}f$ ) through the  $t$ -channel exchange of mediating particles, which necessarily are also charged.

The suppression of the  $s$ -wave annihilation cross section in the chiral limit ( $m_f/m_\chi \rightarrow 0$ ) can be understood from the conservation of angular momentum (see, for example, [6]). Since the initial state consists of two identical fermions, it must be totally anti-symmetric, implying that the  $L = 0$  initial state must also have  $S = 0, J = 0$ . The  $\bar{f}f$  final state must then also have  $J_z = 0$ , where we take the  $z$ -axis to be the direction of motion of the outgoing particles. This outgoing state necessarily has  $L_z = 0$ , implying  $S_z = 0$ . So the outgoing fermion and anti-fermion have the same helicity, and must arise from different Weyl spinors. The  $s$ -wave annihilation matrix element thus violates Standard Model flavor symmetries in the chiral limit, and must be proportional to the Weyl spinor mixing introduced by new physics. As a result,  $s$ -wave annihilation is suppressed in scenarios such as MFV, where Weyl spinor mixing vanishes in the chiral limit.

The  $L = 1$  initial state, however, can have  $S = 1, J = 1$ ; the  $J = 1$  fermion/anti-fermion final state can have  $S_z = J_z = 1$ , implying that the fermion and anti-fermion have opposite helicities and arise from the same Weyl spinor. Thus, the  $p$ -wave annihilation matrix element survives in the chiral limit even if there is no Weyl spinor mixing.

However, the  $s$ -wave dark matter initial state can annihilate to a fermion/anti-fermion pair if an additional photon is also emitted. In this case, the annihilation matrix element survives in the chiral limit; the  $\bar{f}f\gamma$  final state can have  $J = 0$  even if  $f$  and  $\bar{f}$  arise from the same Weyl spinor, due to the angular momentum carried by the photon. Similarly, the  $s$ -wave dark matter initial state can annihilate to a  $\gamma\gamma$  final state through a one-loop diagram with  $f$  and charged mediators running in the loop; this amplitude also survives in the chiral limit (see Figure 2).

In general, we can express the fermion-photon vertex as

$$\Gamma^\mu(q^2) = \gamma^\mu F_1(q^2) + \frac{i\sigma^{\mu\nu}q_\nu}{2m} F_2(q^2) + \frac{i\sigma^{\mu\nu}\gamma^5 q_\nu}{2m} F_3(q^2) + (\gamma^\mu q^2 - \not{q}q^\mu)\gamma^5 F_A(q^2), \quad (1)$$

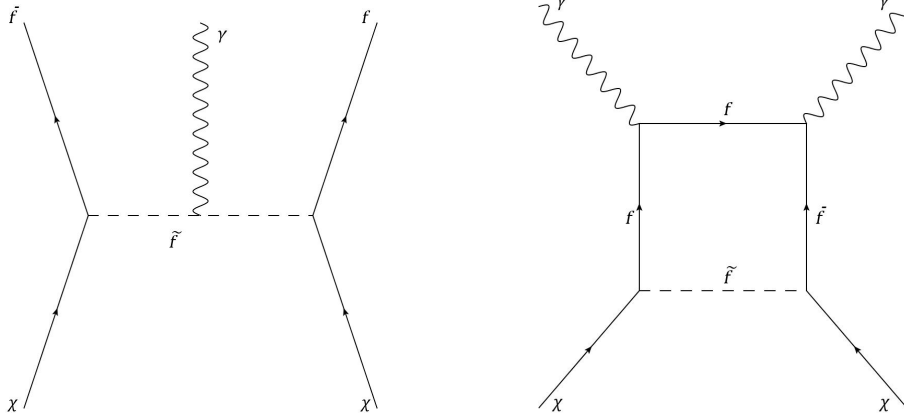


FIG. 2: Representative Feynman diagrams corresponding to the annihilation processes  $\chi\chi \rightarrow \bar{f}f\gamma$  (left diagram) and  $\chi\chi \rightarrow \gamma\gamma$  (right diagram).

where  $q$  is the photon momentum and the  $F_{1,2,3,A}$  are form factors. The form factors can receive contributions from new physics, including one-loop vertex correction diagrams where  $\chi$  and the charged mediators run in the loop. One can classify these form factors based on the transformation properties of the various vertex correction terms under  $C$ ,  $P$ , and SM flavor symmetries. In particular,  $F_2$  and  $F_3$  violate SM flavor symmetries by mixing SM Weyl spinors; they must vanish in the chiral limit if there is no Weyl spinor mixing. Both  $F_1$  and  $F_2$  are invariant under  $C$  and  $P$  separately, while  $F_3$  is  $CP$ -odd.  $F_A$  is  $CP$ -even, but is odd under  $C$  and  $P$  individually.

We can thus make a general connection between corrections to the various form factors and terms in the  $\chi\chi \rightarrow \bar{f}f, \bar{f}f\gamma, \gamma\gamma$  annihilation matrix elements in the chiral limit. The non-relativistic  $s$ -wave annihilation matrix element for the process  $\chi\chi \rightarrow \bar{f}f$  is necessarily proportional to Weyl spinor mixing, so these terms will be related to corrections to the  $F_2$  and  $F_3$  form factors, and specifically to corrections to the magnetic and electric dipole moments [1]. In particular, the  $CP$ -conserving term of the  $s$ -wave annihilation matrix element is related to the correction to magnetic dipole moment, while the  $CP$ -violating term is related to the electric dipole moment correction. But these terms vanish in the chiral limit if there is no Weyl spinor mixing.

If there is no Weyl spinor mixing, and if  $C$  and  $P$  are separately conserved, then the only form factor which can receive a correction is  $F_1$ . This correction is then related to the annihilation matrix elements which do not mix SM fermion Weyl spinors, in particular, the  $p$ -wave matrix element for the process  $\chi\chi \rightarrow \bar{f}f$  and the  $s$ -wave matrix elements for the processes  $\chi\chi \rightarrow \bar{f}f\gamma, \gamma\gamma$ .<sup>1</sup>

<sup>1</sup> Note, we do not consider the  $p$ -wave matrix elements for the processes  $\chi\chi \rightarrow \bar{f}f\gamma, \gamma\gamma$ , since they are always suppressed, compared to their  $s$ -wave counterparts.

We can implement the scenario described above with a simplified model, in which  $\chi$  is a gauge-singlet Majorana fermion which couples to a single Standard Model fermion  $f$  through the exchange of two scalars,  $\tilde{f}_L$  and  $\tilde{f}_R$ , via the Lagrangian

$$\mathcal{L}_f = \lambda_f \tilde{f}_L (\bar{\chi} P_L f) + \lambda_f \tilde{f}_R (\bar{\chi} P_R f) + h.c., \quad (2)$$

where  $\lambda_f$  is a real dimensionless coupling constant. We assume that  $\chi$  and  $\tilde{f}_{L,R}$  are odd under a  $Z_2$  symmetry which stabilizes the dark matter. The  $\tilde{f}_{L,R}$  have the same quantum numbers as left- and right-handed sfermions. We further assume that  $\tilde{f}_L$  and  $\tilde{f}_R$  do not mix and have the same mass ( $m_{\tilde{f}} \equiv m_{\tilde{f}_L} = m_{\tilde{f}_R}$ ). These choices ensure that the annihilation matrix elements respect  $C$  and  $P$ , and do not mix SM Weyl spinors in the chiral limit.

Note, for simplicity, we have assumed that the dominant dark matter coupling is to a single Standard Model fermion. Of course, since  $\tilde{f}_L$  is a member of an  $SU(2)_L$  doublet, it has a corresponding partner, with a different charge, which we may denote by  $\tilde{f}'_L$ . One could embed the coupling of this field to dark matter within a  $C$ - and  $P$ -invariant theory by adding a copy of the interaction Lagrangian in eq. (2),

$$\mathcal{L}_{f'} = \lambda_{f'} \tilde{f}'_L (\bar{\chi} P_L f') + \lambda_{f'} \tilde{f}'_R (\bar{\chi} P_R f') + h.c., \quad (3)$$

where  $f'$  is a fermion in the same generation as  $f$ ,  $\tilde{f}'_{L,R}$  is another scalar field, and  $\lambda_{f'}$  is a dimensionless coupling. For most of the quantities which we will consider there will be no interference between the terms in  $\mathcal{L}_f$  and  $\mathcal{L}_{f'}$ . In particular, corrections to the fermion-photon vertex for  $f$ , and the cross sections for the processes  $\chi\chi \rightarrow \bar{f}f$  and  $\chi\chi \rightarrow \bar{f}f\gamma$ , are unchanged, while similar processes involving  $f'$  depend only on the interactions contained in  $\mathcal{L}_{f'}$ . But the cross section for the process  $\chi\chi \rightarrow \gamma\gamma$  will depend on all of these terms, since  $f$  and  $f'$  can both run in the loop; note, though, even this consideration is not relevant if  $f$  is a charged lepton, since  $f'$  and  $\tilde{f}'_{L,R}$  are then electrically neutral and do not couple to the photon.

One could also consider the case where  $\tilde{f}_{L,R}$  couples to multiple fermions in different generations, but in this case, there can also be contributions to tightly constrained flavor-changing processes, such as  $f_1 \rightarrow f_2\gamma$ , through diagrams where  $\tilde{f}_{L,R}$  and  $\chi$  run in the loop. As a result, one might expect only the coupling of  $\tilde{f}_{L,R}$  to one of the fermions to be dominant. We will discuss the effect on this analysis if dark matter couples to multiple fermions in the next section.

## 2.1. Annihilation

To lowest order in the relative velocity ( $v$ ), the annihilation cross section for the process  $\chi\chi \rightarrow \bar{f}f$  can be written as (see, for example, [7–9])

$$\langle\sigma_{\bar{f}f}v\rangle = \frac{\lambda_f^4 N_c r}{12\pi m_{\bar{f}}^2} \frac{1+r^2}{(1+r)^4} \langle v^2 \rangle, \quad (4)$$

where  $\langle v^2 \rangle$  is the thermal average of  $v^2$  and  $r \equiv m_\chi^2/m_{\bar{f}}^2$  satisfies the constraint  $0 < r \leq 1$ . Since there is no Weyl spinor mixing, this cross section is necessarily  $p$ -wave suppressed.  $N_c$  is the number of color states for the fermion  $f$ ;  $N_c = 1$  if  $f = e, \mu, \tau$ , while  $N_c = 3$  if  $f = q$ . If the dark matter is a thermal relic, then at the time of freeze-out, one expects  $\langle v^2 \rangle \sim 0.1$ . But in the current epoch,  $\langle v^2 \rangle \sim 10^{-6}$ , implying that the  $\bar{f}f\gamma$  and  $\gamma\gamma$  final states may be important for the purposes of indirect detection.

The differential cross section for the process  $\chi\chi \rightarrow \bar{f}f\gamma$  can be written as [10, 11]

$$\begin{aligned} \frac{d\sigma_{\bar{f}f\gamma}}{dx} v &= \frac{\lambda_f^4 N_c \alpha Q_f^2 r (1-x)}{32\pi^2 m_{\bar{f}}^2} \left[ \frac{4x}{(1+r)(1+r-2xr)} - \frac{2x}{(1+r-xr)^2} \right. \\ &\quad \left. + \frac{(1+r)(1+r-2xr)}{r(1+r-xr)^3} \ln \frac{1+r-2xr}{1+r} \right], \end{aligned} \quad (5)$$

where  $Q_f$  is the electric charge of  $f$ ,  $x \equiv E_\gamma/m_\chi$ ,  $E_\gamma$  is the energy of the photon, and  $0 \leq x \leq 1$ . The total cross section is then given by [7, 11, 12]

$$\begin{aligned} \langle\sigma_{\bar{f}f\gamma}v\rangle &= \frac{\lambda_f^4 N_c \alpha Q_f^2}{32\pi^2 m_{\bar{f}}^2 r^2} \left[ (1+r) \left( \frac{\pi^2}{6} - \ln^2 \frac{1+r}{2} - 2\text{Li}_2 \frac{1+r}{2} \right) \right. \\ &\quad \left. + \frac{3r^2+4r}{1+r} + \frac{4-3r-r^2}{2} \ln \frac{1-r}{1+r} \right]. \end{aligned} \quad (6)$$

We are primarily interested in the limits  $r \sim 1$  (when the  $\chi$  has nearly the same mass as the mediators) and  $r \ll 1$  (when the mediators are heavy). We then find

$$\begin{aligned} \langle\sigma_{\bar{f}f\gamma}v\rangle_{r \ll 1} &\sim \frac{\lambda_f^4 N_c r}{120\pi^2 m_{\bar{f}}^2} (\alpha Q_f^2 r^2), \\ \langle\sigma_{\bar{f}f\gamma}v\rangle_{r \rightarrow 1} &\sim \frac{\lambda_f^4 N_c}{32\pi^2 m_{\bar{f}}^2} \left[ \frac{7}{2} - \frac{\pi^2}{3} \right] \alpha Q_f^2. \end{aligned} \quad (7)$$

The total cross section for the one-loop process  $\chi\chi \rightarrow \gamma\gamma$  can be written as [11, 13–15]

$$\langle\sigma_{\gamma\gamma}v\rangle = \frac{\lambda_f^4 N_c^2 \alpha^2 Q_f^4}{64\pi^3 m_{\bar{f}}^2 r} [\text{Li}_2(r) - \text{Li}_2(-r)]^2, \quad (8)$$

yielding

$$\begin{aligned}\langle\sigma_{\gamma\gamma}v\rangle_{r\ll 1} &\sim \frac{\lambda_f^4 N_c^2 r}{16\pi^3 m_{\tilde{f}}^2} \alpha^2 Q_f^4, \\ \langle\sigma_{\gamma\gamma}v\rangle_{r\rightarrow 1} &\sim \frac{\lambda_f^4 N_c^2 \pi}{1024 m_{\tilde{f}}^2} \alpha^2 Q_f^4.\end{aligned}\tag{9}$$

## 2.2. Correction to the Form Factor

One can also compute the vertex correction arising from the two diagrams where  $\chi$  and either  $\tilde{f}_L$  or  $\tilde{f}_R$  run in the loop. As expected, the only form factor which receives a correction is  $F_1$ . To first order in  $q^2$ ,  $F_1$  is often represented by the expansion

$$F_1(q^2) \equiv 1 + \frac{1}{6} q^2 R^2 + \mathcal{O}(q^4),\tag{10}$$

where  $R$  is referred to as the charge radius (gauge-invariance implies that  $F_1(q^2 = 0) = 1$ ). In a non-Abelian gauge theory, however, this quantity is not necessarily gauge-invariant for  $q^2 \neq 0$  [2–4], leading to ambiguity in the meaning of the charge radius. For example, if one computed in an  $R_\xi$ -gauge, one would find that, although the diagram in the right panel of Figure 1 is  $\xi$ -independent (as it contains no gauge bosons in the loop), there are other vertex corrections involving Standard Model fields which are  $\xi$ -dependent; the  $\xi$ -dependence cancels when computing an observable quantity, such as an  $S$ -matrix element.

But the vertex correction arising from the diagram in Figure 1 (right panel) yields a correction to  $F_1$  which is gauge-invariant, and can be parameterized as

$$\Delta F_1(q^2) = \frac{1}{6} q^2 \Delta R^2 + \mathcal{O}(q^4).\tag{11}$$

The  $\mathcal{O}(q^0)$  term in the correction is necessarily canceled by the fermion external leg correction, as guaranteed by the Ward-Takahashi identity. The parameter  $\Delta R$  may be thought of heuristically as a correction to the charge radius, but it is more precisely a parameter which can be extracted from cross sections.

This correction is given by

$$|\Delta R^2| = \frac{3\lambda_f^2}{8\pi^2 m_{\tilde{f}}^2} \frac{3r^2 + (1 - 4r) - 2r^2 \ln r}{4(1 - r)^3}.\tag{12}$$

Again, our main interest is in the limits  $r \sim 1$  and  $r \ll 1$ , in which case we find

$$\begin{aligned} |\Delta R^2|_{r \ll 1} &= \frac{3\lambda_f^2}{32\pi^2 m_{\tilde{f}}^2}, \\ |\Delta R^2|_{r \sim 1} &= \frac{\lambda_f^2}{16\pi^2 m_{\tilde{f}}^2}. \end{aligned} \quad (13)$$

We thus see that the correction scales

$$\Delta R^2 \propto \lambda_f^2 / m_{\tilde{f}}^2, \quad (14)$$

where the remaining model dependence arises only from rescaling by an  $\mathcal{O}(1)$  function of  $r$ .

We may then express the relevant annihilation cross sections in terms of  $\Delta R^2$  and  $r$  as

$$\begin{aligned} \langle \sigma_{\tilde{f}\tilde{f}} v \rangle &= \left[ N_c (\Delta R^2)^2 m_{\tilde{f}}^2 r \langle v^2 \rangle \right] \left( \frac{256\pi^3}{27} \left( \frac{(1-r)^3}{3r^2 + (1-4r) - 2r^2 \ln r} \right)^2 \left( \frac{1+r^2}{(1+r)^4} \right) \right), \\ \langle \sigma_{\tilde{f}\tilde{f}\gamma} v \rangle &= \left[ N_c (\Delta R^2)^2 m_{\tilde{f}}^2 r^3 \alpha Q_f^2 \right] \left( \frac{32\pi^2}{9} \left( \frac{(1-r)^3}{3r^2 + (1-4r) - 2r^2 \ln r} \right)^2 \left( \frac{1}{r^5} \right) \right) \\ &\quad \times \left[ (1+r) \left( \frac{\pi^2}{6} - \ln^2 \frac{1+r}{2} - 2\text{Li}_2 \frac{1+r}{2} \right) + \frac{3r^2 + 4r}{1+r} + \frac{4 - 3r - r^2}{2} \ln \frac{1-r}{1+r} \right], \\ \langle \sigma_{\gamma\gamma} v \rangle &= \left[ N_c^2 (\Delta R^2)^2 m_{\tilde{f}}^2 r \alpha^2 Q_f^4 \right] \left( \frac{16\pi}{9} \left( \frac{(1-r)^3}{3r^2 + (1-4r) - 2r^2 \ln r} \right)^2 \right) \left[ \frac{\text{Li}_2(r) - \text{Li}_2(-r)}{r} \right]^2 \end{aligned} \quad (15)$$

All of these annihilation cross sections scale with  $\Delta R^2$  and the mediator mass as  $\langle \sigma v \rangle \propto (\Delta R^2)^2 m_{\tilde{f}}^2$ ; constraints on the annihilation cross section thus become weaker if the mediating particles are heavy. But the cross sections for the processes  $\chi\chi \rightarrow \tilde{f}\tilde{f}, \tilde{f}\tilde{f}\gamma, \gamma\gamma$  scale as  $r, r^3, r$ , respectively. These constraints are thus most stringent when the dark matter is much lighter than the mediator, and the mediator is as light as is consistent with experimental constraints.

Note, we have assumed that dark matter couples to only one SM fermion, so there are no interference effects. If dark matter couples to multiple SM fermions  $f_i$ , then the connection between  $\Delta R^2$  for the fermion  $f_i$  and the cross sections  $\langle \sigma_{\tilde{f}_i \tilde{f}_i} v \rangle$  and  $\langle \sigma_{\tilde{f}_i \tilde{f}_i \gamma} v \rangle$  is unchanged, since in each case only  $f_i$  appears in the relevant diagrams. However, for the loop diagrams which contribute to the process  $\chi\chi \rightarrow \gamma\gamma$ , all of the  $f$ s can run in the loop.

We can consider the simple generalization in which, each SM fermion  $f_i$  couples to  $\chi$  via an interaction with the scalars  $\tilde{f}_{L_i, R_i}$ , with coupling  $\lambda_{f_i}$ . Assuming that  $m_{f_i} \ll m_\chi, m_{\tilde{f}_i}$  for all  $i$ , then we find (generalizing the result from [11])

$$\langle \sigma_{\gamma\gamma} v \rangle = \frac{\alpha^2}{64\pi^3 m_\chi^2} \left( \sum_i \lambda_{f_i}^2 N_{C(i)} Q_{f_i}^2 [\text{Li}_2(r_i) - \text{Li}_2(-r_i)] \right)^2, \quad (16)$$

where  $r_i = m_\chi^2 / m_{\tilde{f}_i}^2$ .

### 3. CONSTRAINTS FROM DATA

We have found relationships between dark matter annihilation cross sections and the vertex correction diagram given in Figure 1 (right panel), but in order to constrain the vertex correction, it is necessary to relate it to observables. This is non-trivial because in a non-Abelian gauge theory, such as the Standard Model,  $F_1(q^2)$  need not be gauge-invariant if  $q^2 \neq 0$  [2–4]. However, the gauge-dependence cancels when computing an observable quantity, such as an  $S$ -matrix element. We will see that the correction given by the diagram in the right panel of Figure 1, and in particular, the parameter  $\Delta R^2$ , can be extracted from observable cross sections.

For simplicity and concreteness, we will focus on the case where  $f = \mu$ . The vertex correction can be extracted from two cross sections: the cross sections for the process  $e^+e^- \rightarrow \bar{\mu}\mu$  and for the process  $e^+e^- \rightarrow \bar{\tau}\tau$ , for example. At tree-level, both processes are mediated by neutral gauge boson ( $\gamma, Z$ ) exchange in the  $s$ -channel (we may neglect Higgs boson exchange, as the coupling of the Higgs boson to the electron is very small). If we take the limit  $m_{\tau,\mu} \ll s$ , then the Standard Model cross section is flavor independent:

$$\sigma_{e^+e^- \rightarrow \bar{\mu}\mu}^{SM} = \sigma_{e^+e^- \rightarrow \bar{\tau}\tau}^{SM}, \quad (17)$$

If we include the new fields and interactions encoded in  $\mathcal{L}_{f=\mu}$ , then we find two new classes of one-loop diagrams which can contribute to these processes. These are diagrams where a neutral gauge boson is exchanged in the  $s$ -channel and either a) the gauge boson two-point function is corrected by  $\tilde{f}_{L,R}$  running in a loop, or b) the muon vertex or propagator is corrected by a  $\tilde{f}_{L,R}$  and  $\chi$  running in the loop. The first set of diagrams provide the same correction to the matrix element for  $e^+e^- \rightarrow \bar{\mu}\mu$  and  $e^+e^- \rightarrow \bar{\tau}\tau$ . But the vertex and fermion propagator correction diagrams affect only the cross section for  $e^+e^- \rightarrow \bar{\mu}\mu$ , so the correction to the vertex can be extracted from a search for a deviation from lepton universality.

The effect of the muon vertex and propagator corrections on the annihilation matrix element can be parameterized by a  $q^2$ -dependent shift of the muon charge parameter, as it appears in the tree-level matrix element:

$$\delta Q_\mu = Q_\mu \left( \frac{1}{6} q^2 \Delta R^2 + \mathcal{O}(q^4 \Delta R^4) \right), \quad (18)$$

where  $q^2 = s$  and  $Q_\mu$  is the muon charge. We do not mean to say that the charge is scale-dependent; this is just a convenient way to express this set of one-loop diagrams in terms of the tree-level diagrams by absorbing the correction into the coefficient of the vertex. The Ward-Takahashi identity ensures that, after including both the vertex and propagator correction, the

shift vanishes at  $q^2 = 0$ . Note that the vertex correction does not simply rescale the cross section, because the  $Z$  couples to the muon via a  $V - A$  coupling, and the vertex correction associated with  $\chi, \tilde{f}_{L,R}$  only affects the vector interaction.

If we assume that the one loop corrections are small, then the vertex correction diagram only affects the cross section through interference with the tree-level matrix element. We thus find

$$\sigma_{e^+e^- \rightarrow \bar{\mu}\mu}^{1-loop} - \sigma_{e^+e^- \rightarrow \bar{\tau}\tau}^{1-loop} \approx \left( \sigma_{e^+e^- \rightarrow \bar{\mu}\mu}^{SM(tree)} \right)_{Q_\mu \rightarrow Q_\mu(1+q^2\Delta R^2/6)} - \sigma_{e^+e^- \rightarrow \bar{\mu}\mu}^{SM(tree)}. \quad (19)$$

The left hand side of this relation involves cross sections calculated at one-loop, including the effects of new physics, and can be measured or constrained using collider data. The right hand side is a function of the parameter  $\Delta R^2$  and of tree-level SM cross sections which can be easily computed, allowing one to extract  $\Delta R^2$  from data.

Although we focus specifically on the case where  $f = \mu$ , and on extracting the parameter  $\Delta R^2$  from the processes  $e^+e^- \rightarrow \bar{\mu}\mu, \bar{\tau}\tau$ , this strategy can clearly be generalized to other choices of  $f$ , and to other initial states, such as  $e^-q$ . We will comment in the Conclusions on more complicated scenarios, in which extracting the correction unambiguously may not be as easy.

### 3.1. Collider Results

Searches for sleptons have been performed at LEP [16–19] and the LHC [20, 21], and can be used to place rough lower bounds on  $m_{\tilde{f}}$  in the case where  $f = e, \mu, \tau$ . Consistency with searches at LEP require  $m_{\tilde{f}} \gtrsim 100 \text{ GeV}$ , while LHC searches would require  $m_{\tilde{f}} \gtrsim 300 \text{ GeV}$  in the  $r \rightarrow 0$  limit (these constraints are a little weaker in the  $r \rightarrow 1$  limit). In the case where  $f = q$ , one can estimate lower bounds on  $m_{\tilde{f}}$  from LHC squark searches [22]. These bounds would roughly require  $m_{\tilde{f}} \gtrsim 500 \text{ GeV}$  in the  $r \rightarrow 0$  limit (again, these constraints are somewhat weaker in the  $r \rightarrow 1$  limit). As shown in eq. (15), bounds on the dark matter annihilation cross sections are strongest when  $m_{\tilde{f}}$  saturates the lower bound.

LEP has made precise measurements of the energy dependence of the  $e^+e^- \rightarrow \bar{f}f$  cross section [5]. For the LEP analysis,  $f = e, \mu, \tau$ , or  $q$ , where  $q = u, d, s, c, b$  (it was assumed that quarks have identical vertex functions). The correction to the cross section was parameterized by

$$\frac{d\sigma_{e^+e^- \rightarrow \bar{f}f}}{dq^2} = \frac{d\sigma_{e^+e^- \rightarrow \bar{f}f}^{SM}}{dq^2} \left( 1 + \frac{q^2\Delta R^2}{6} \right)^4. \quad (20)$$

These constraints on  $|\Delta R|$  are summarized in Table I.

Note, it was assumed that the electron and outgoing fermion vertex functions received the same correction; these constraints are thus weakened for  $f \neq e$  by a factor  $\sqrt{2}$  if the electron is instead

channel	$ \Delta R $
$e^+e^-$	$< 3.1 \times 10^{-19}\text{m}$
$\mu^+\mu^-$	$< 2.4 \times 10^{-19}\text{m}$
$\tau^+\tau^-$	$< 4.0 \times 10^{-19}\text{m}$
$\bar{q}q$	$< 3.0 \times 10^{-19}\text{m}$

TABLE I: Constraints on the parameter  $|\Delta R|$  for Standard Model fermions ( $e, \mu, \tau$ ) and quarks ( $q$ ) obtained from searches at LEP [5], using the parametrization discussed in the text.

taken to be point-like. Comparable constraints on the correction to the quark vertex functions have been obtained at HERA [23], using a similar parametrization.

If  $m_{\tilde{f}} \gtrsim 300 \text{ GeV}$ , then a value of  $\Delta R^2$  large enough to be constrained by LEP data would already be close to (if not ruled out by) the perturbativity limit,  $\lambda_f \leq \sqrt{4\pi}$ . It is thus already clear that, given the constraints on charged mediators from the LHC, current bounds from LEP can only be of limited utility in constraining dark matter annihilation.

The parametrization used by LEP for the correction to the cross section is different from the one which we have used, implying that their constraints cannot directly be translated into bounds on dark matter annihilation. However, LEP bounds the deviation of the cross section from the Standard Model prediction; given that their bounds on the deviations of the  $e^+e^- \rightarrow \bar{\mu}\mu$  and  $\rightarrow \bar{\tau}\tau$  cross sections are similar to each other, the deviation of these cross sections from each other cannot be much larger than the deviation from the SM prediction. The bound on the parameter  $\Delta R^2$  for the muon, as we have parametrized it, thus cannot be much larger than that found by LEP using their parametrization. In any case, this bound is already too weak to usefully constrain dark matter annihilation. But future analyses at experiments with higher energy and luminosity could yield much more precise measurements of these cross sections.

For the remainder of this section, we continue to focus on the case  $f = \mu, m_{\tilde{f}} = 300 \text{ GeV}$  and consider two different scenarios: bounds on  $\Delta R$  for the muon at the level given by LEP, and the possibility that the bound on  $\Delta R$  could be improved by a factor of 10 with future experiments. Since the annihilation cross section bounds arising from collider measurements scale as  $\langle \sigma_{\tilde{f}\tilde{f}, \tilde{f}\tilde{f}\gamma, \gamma\gamma} v \rangle \propto (\Delta R)^4 m_{\tilde{f}}^2$ , one can easily rescale these bounds for a different choice of  $m_{\tilde{f}}$ , or for future constraints on  $\Delta R$ . Similarly, the maximum cross section consistent with perturbativity (for any of the channels we have discussed) scales as  $\propto m_{\tilde{f}}^{-2}$ ; one can easily rescale the perturbativity limit for a different choice of  $m_{\tilde{f}}$ .

### 3.2. Thermal Freeze-out

At the time of dark matter thermal freeze-out, one typically expects [24]  $\langle v^2 \rangle \sim \mathcal{O}(0.1)$ . We can express the  $\chi\chi \rightarrow \bar{f}f$   $p$ -wave annihilation cross section as

$$\begin{aligned} \langle \sigma_{\bar{f}f} v \rangle &= (5.5 \times 10^3 \text{ pb}) r N_c \left[ \left( \frac{\Delta R^2}{(3 \times 10^{-19} \text{ m})^2} \right)^2 \left( \frac{m_{\tilde{f}}}{300 \text{ GeV}} \right)^2 \frac{\langle v^2 \rangle}{0.1} \right] \\ &\times \left( \frac{(1-r)^3}{3r^2 + (1-4r) - 2r^2 \ln r} \right)^2 \left( \frac{(1+r^2)}{(1+r)^4} \right). \end{aligned} \quad (21)$$

In Figure 3, we plot the constraints on  $\langle \sigma_{\bar{f}f} v \rangle$  as a function of  $r$  ( $m_{\tilde{f}} = 300 \text{ GeV}$ ,  $\langle v^2 \rangle = 0.1$ ). The red long-dashed contour describes the constraints which arise from LEP bounds on  $\Delta R$  for the muon, while the blue short-dashed contour describes the constraints which would arise if  $\Delta R$  were constrained to be 10 times smaller by future data. The regions above the contours are excluded, assuming that there is no other source for vertex corrections. Also plotted is the largest cross section consistent with perturbativity ( $\lambda_f^2 = 4\pi$ ). We see that, if the precision of constraints on  $\Delta R$  can reach the  $\mathcal{O}(10^{-20} \text{ m})$  level for  $m_{\tilde{f}} \lesssim 3000 \text{ GeV}$ , then models in which the dark matter relic density in early Universe is depleted by two-body  $p$ -wave annihilation would be correlated with a measurable energy-dependent deviation from lepton universality.

### 3.3. Indirect Detection in the Current Epoch

In the current epoch, when  $\langle v^2 \rangle \sim 10^{-6}$ , indirect detection signals arising from the processes  $\chi\chi \rightarrow \bar{f}f\gamma$  (internal bremsstrahlung) and  $\chi\chi \rightarrow \gamma\gamma$  (via a one-loop diagram) may be competitive with  $\chi\chi \rightarrow \bar{f}f$ . We may express these annihilation cross sections as

$$\begin{aligned} \langle \sigma_{\bar{f}f\gamma} v \rangle &= (12.8 \text{ pb}) r^3 N_c Q_f^2 \left[ \left( \frac{\Delta R^2}{(3 \times 10^{-19} \text{ m})^2} \right)^2 \left( \frac{m_{\tilde{f}}}{300 \text{ GeV}} \right)^2 \right] \\ &\times \left( \frac{15}{4} \left( \frac{(1-r)^3}{3r^2 + (1-4r) - 2r^2 \ln r} \right)^2 \left( \frac{1}{r^5} \right) \right) \\ &\times \left[ (1+r) \left( \frac{\pi^2}{6} - \ln^2 \frac{1+r}{2} - 2\text{Li}_2 \frac{1+r}{2} \right) + \frac{3r^2 + 4r}{1+r} + \frac{4-3r-r^2}{2} \ln \frac{1-r}{1+r} \right], \\ \langle \sigma_{\bar{\gamma}\gamma} v \rangle &= (0.22 \text{ pb}) r N_c^2 Q_f^4 \left[ \left( \frac{\Delta R^2}{(3 \times 10^{-19} \text{ m})^2} \right)^2 \left( \frac{m_{\tilde{f}}}{300 \text{ GeV}} \right)^2 \right] \\ &\times \left( \frac{(1-r)^3}{3r^2 + (1-4r) - 2r^2 \ln r} \right)^2 \left( \frac{\text{Li}_2(r) - \text{Li}_2(-r)}{2r} \right)^2. \end{aligned} \quad (22)$$

Note, even though we might expect that  $\chi$  couples to  $\nu_\mu$  through interactions with the other member of the  $SU(2)_L$  doublet of which  $\tilde{f}_L$  is a member, those interactions will not contribute to

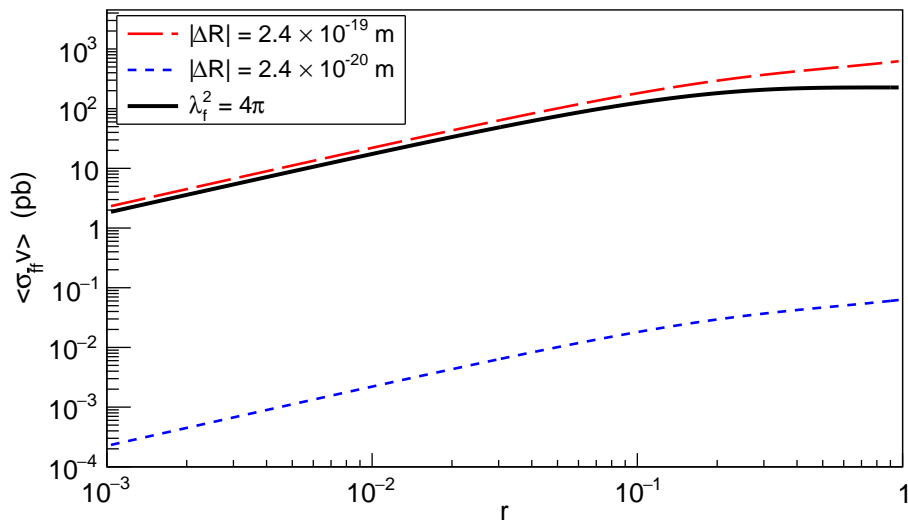


FIG. 3: Bounds on  $\langle \sigma_{\bar{f}f} v \rangle$  (in pb) arising from measurements of  $\Delta R$ , where  $f = \mu$ ,  $m_{\bar{f}} = 300$  GeV and  $\langle v^2 \rangle = 0.1$ . The red long-dashed contour corresponds to the case where  $\Delta R = 2.4 \times 10^{-19}$  m (the current limit reported by LEP [5]), and the blue short-dashed contour corresponds to the case where  $\Delta R = 2.4 \times 10^{-20}$  m. The region above the curves is excluded, if there are no other corrections arising from new physics unconnected to the model we have discussed. Also shown is the perturbativity limit,  $\lambda_f^2 = 4\pi$  (black solid).

$\chi\chi \rightarrow \gamma\gamma$ , since neutrinos are electrically neutral.

In Figures 4 and 5, we plot the constraints on  $\langle \sigma_{\gamma\gamma} v \rangle$  and  $\langle \sigma_{\bar{f}f\gamma} v \rangle$ , respectively, as functions of  $r$  ( $m_{\bar{f}} = 300$  GeV). The red long-dashed contour describes the constraints which arise from current LEP bounds on  $\Delta R$  for the muon, while the blue short-dashed contour describes the constraints which would arise if  $\Delta R$  were constrained to be 10 times smaller by future data. Again, the regions above the contours are excluded if there are no other sources for corrections to the vertex, and we also plot the largest cross sections consistent with perturbativity ( $\lambda_f^2 = 4\pi$ ). In Figure 4, we also plot current observational bounds on  $\langle \sigma_{\gamma\gamma} v \rangle$  obtained by Fermi-LAT [26].

The process  $\chi\chi \rightarrow \gamma\gamma$  can proceed from an  $s$ -wave initial state, but  $\langle \sigma_{\gamma\gamma} v \rangle$  is suppressed by a factor  $\alpha^2 \sim \mathcal{O}(10^{-4})$ . This cross section will be somewhat larger than  $\langle \sigma_{\bar{f}f} v \rangle$  in the current epoch. Moreover, because this annihilation process produces monoenergetic photons, the signal is much more easily detected above background. As a result, this process will be much more important than  $\chi\chi \rightarrow \bar{f}f$  for indirect detection in the current epoch. For  $m_{\bar{f}} \sim 300$  GeV, we find that constraints on the  $\chi\chi \rightarrow \gamma\gamma$  annihilation process arising from collider probes of  $\Delta R$  could exceed current constraints from Fermi-LAT by more than three orders of magnitude (absent fine-tuning),

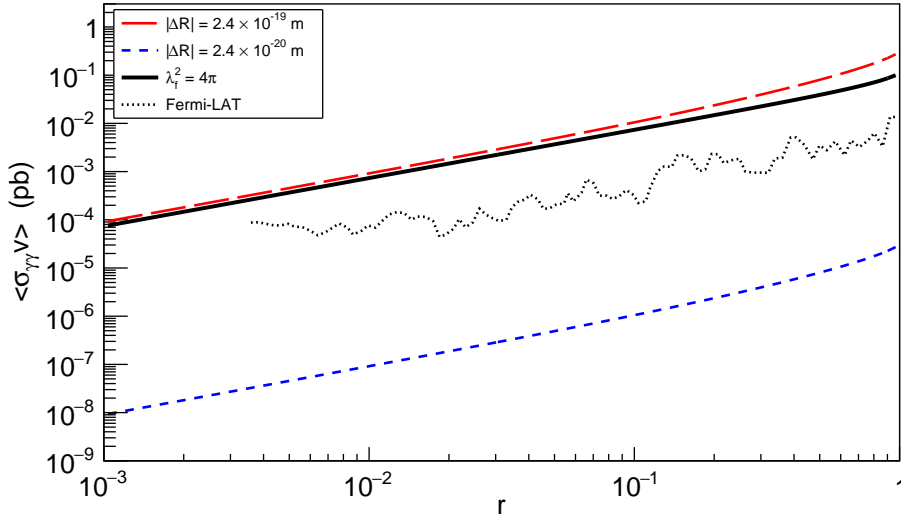


FIG. 4: Bounds on  $\langle \sigma_{\bar{f}f} v \rangle$  (in pb) arising from measurements of  $\Delta R$ , where  $f = \mu$  and  $m_{\bar{f}} = 300$  GeV. The red long-dashed contour corresponds to the case where  $\Delta R = 2.4 \times 10^{-19}$  m (the current limit reported by LEP [5]), and the blue short-dashed contour corresponds to the case where  $\Delta R = 2.4 \times 10^{-20}$  m. The region above the curves is excluded, if there are no other corrections arising from new physics unconnected to the model we have discussed. Also shown is the perturbativity limit (black solid), and observational bounds from Fermi-LAT (black dotted) [26].

if  $\Delta R$  could be constrained at the  $\mathcal{O}(10^{-20})$  m level.

Dark matter annihilation via internal bremsstrahlung is an  $s$ -wave process, but instead receives a factor  $\alpha r^2$  suppression. For  $r \sim 1$ , however, the photon spectrum arising from internal bremsstrahlung is very hard; the photon spectrum is similar in shape to a line signal, implying that the IB cross section can also be constrained by line signal searches using Fermi-LAT [26]. For  $m_{\bar{f}} \sim 300$  GeV, constraints on  $\langle \sigma_{\bar{f}f} v \rangle$  arising from collider probes of  $\Delta R$  could surpass Fermi-LAT constraints on IB in the nearly-degenerate limit by up to two orders of magnitude, if  $\Delta R$  can be constrained at the  $\mathcal{O}(10^{-20})$  m level.

For  $r < 1$ , however, the photon spectrum will be smooth, and the sensitivity of Fermi-LAT and other indirect detection experiments will be significantly weaker. Measurements of  $\Delta R$  at the  $\mathcal{O}(10^{-20})$  m level would thus provide an even more dramatic improvement over current indirect detection results. But for  $r \lesssim \mathcal{O}(0.1)$ , however, we see that indirect detection prospects will in any case tend to be dominated by the process  $\chi\chi \rightarrow \gamma\gamma$ .

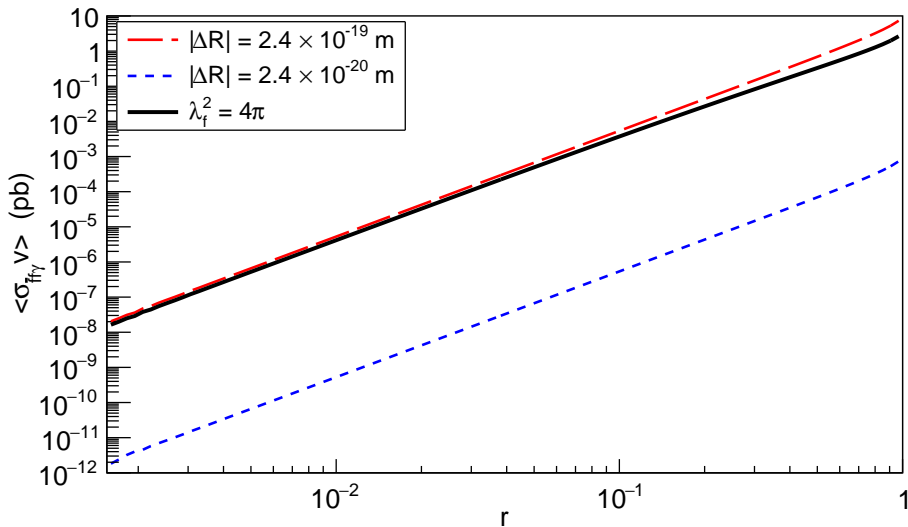


FIG. 5: Bounds on  $\langle \sigma_{\bar{f}f\gamma} v \rangle$  (in pb) arising from measurements of  $\Delta R$ , where  $f = \mu$  and  $m_{\bar{f}} = 300$  GeV. The red long-dashed contour corresponds to the case where  $\Delta R = 2.4 \times 10^{-19}$  m (the current limit reported by LEP [5]), and the blue short-dashed contour corresponds to the case where  $\Delta R = 2.4 \times 10^{-20}$  m. The region above the curves is excluded, if there are no other corrections arising from new physics unconnected to the model we have discussed. Also shown is the perturbativity limit (black solid).

#### 4. CONCLUSIONS

We have seen that probes of Standard Model fermion form factor corrections can be used to constrain cross sections for dark matter annihilation in scenarios where dark matter couples to SM fermions through charged mediators, and where helicity mixing is suppressed. In particular, the  $p$ -wave cross section for the process  $\chi\chi \rightarrow \bar{f}f$ , and  $s$ -wave cross sections for the internal bremsstrahlung process  $\chi\chi \rightarrow \bar{f}f\gamma$  and the one-loop process  $\chi\chi \rightarrow \gamma\gamma$ , can be constrained by probes of the corrections to the fermion  $F_1$  form factor, which can be expressed in terms of a parameter  $\Delta R$ . However, it is always possible for other new physics, unrelated to dark matter, to produce canceling corrections to the form factor, allowing a large annihilation cross section to be consistent with experimental data. As such, the bounds we have found do not correspond to a rigorous limit, but rather demarcate the rough point at which fine-tuning would be needed in order to retain consistency with the data.

It is worth noting that the annihilation processes  $\chi\chi \rightarrow \bar{f}f\gamma, \gamma\gamma$  can only proceed if dark matter couples to SM fermions through an interaction mediated by a charged particle. There will thus always be a correction to the fermion-photon vertex arising from a one-loop diagram where dark

matter and the charged mediators run in the loop. Thus, the correlation between the fermion vertex correction and the  $\chi\chi \rightarrow \bar{f}f\gamma, \gamma\gamma$  annihilation cross sections is robust.

Unfortunately, the constraints on the form factor corrections derivable from LEP data are not precise enough to yield useful constraints on dark matter annihilation. But future experiments such as VHEeP [27] and ILC could provide much tighter constraints on the parameter  $\Delta R$ . As the annihilation cross sections scale as  $(\Delta R)^4$ , even a modest improvement in the constraints on  $\Delta R$  would correspond to a dramatic improvement in constraints on the dark matter annihilation cross section. For example, a high-luminosity run at VHEeP could yield an order of magnitude improvement in the measurement of  $\Delta R$  [27], resulting in an improvement in bounds on dark matter annihilation of  $\mathcal{O}(10^{-4})$ . Such a dramatic improvement would result in constraints which essentially exceed all current observational bounds for all of the channels which we have considered over the entire range of  $r$  at  $m_{\bar{f}} \sim 300$  GeV. High-luminosity  $e^+e^-$  colliders would be ideally suited for this type of study [28].

Constraining the parameter  $\Delta R$  requires one to extract the vertex correction contribution due to dark matter from collider data. We have outlined a strategy for the particular case where dark matter couples to muons  $f = \mu$ , but this strategy can be generalized to other choices. However, there are examples where the extraction of the correction from data can be more complicated. For example, if  $f = e$ , then there will be additional one-loop box diagrams which contribute to the  $e^+e^- \rightarrow e^+e^-$  cross section. In this case, one could attempt to extract the vertex correction by searching for a similar deviation from lepton universality with a hadronic initial state ( $\bar{q}q \rightarrow e^+e^-, \bar{\mu}\mu$ ), at high energy and/or high luminosity. However, it is not clear if a similar improvement in the vertex function measurement can be obtained practically.

Finally, one should note that, if future high-energy experiments do indeed find evidence for a sizeable deviation from the Standard Model prediction for the form factor, it could be possible to perform a more detailed analysis of the functional form, beyond simply constraining the first moment.

## 5. ACKNOWLEDGEMENT

We are grateful to Tom Browder, Bhaskar Dutta, Danny Marfatia, Xerxes Tata and Sven Vahsen for useful discussions. JK is supported in part by NSF CAREER grant PHY-1250573.

- 
- [1] K. Fukushima and J. Kumar, Phys. Rev. D **88**, no. 5, 056017 (2013) doi:10.1103/PhysRevD.88.056017 [arXiv:1307.7120].
  - [2] J. L. Lucio, A. Rosado and A. Zepeda, Phys. Rev. D **29**, 1539 (1984). doi:10.1103/PhysRevD.29.1539
  - [3] N. M. Monyonko and J. H. Reid, Prog. Theor. Phys. **73**, 734 (1985). doi:10.1143/PTP.73.734
  - [4] J. Bernabeu, J. Papavassiliou and D. Binosi, Nucl. Phys. B **716**, 352 (2005) doi:10.1016/j.nuclphysb.2005.02.039 [hep-ph/0405288].
  - [5] M. Acciarri *et al.* [L3 Collaboration], Phys. Lett. B **489**, 81 (2000) doi:10.1016/S0370-2693(00)00887-X [hep-ex/0005028].
  - [6] J. Kumar and D. Marfatia, Phys. Rev. D **88**, no. 1, 014035 (2013) doi:10.1103/PhysRevD.88.014035 [arXiv:1305.1611 [hep-ph]].
  - [7] N. F. Bell, J. B. Dent, A. J. Galea, T. D. Jacques, L. M. Krauss and T. J. Weiler, Phys. Lett. B **706**, 6 (2011) doi:10.1016/j.physletb.2011.10.057 [arXiv:1104.3823 [hep-ph]].
  - [8] A. Pierce, N. R. Shah and K. Freese, arXiv:1309.7351 [hep-ph].
  - [9] K. Fukushima, C. Kelso, J. Kumar, P. Sandick and T. Yamamoto, Phys. Rev. D **90**, no. 9, 095007 (2014) doi:10.1103/PhysRevD.90.095007 [arXiv:1406.4903 [hep-ph]].
  - [10] T. Bringmann, L. Bergstrom and J. Edsjo, JHEP **0801**, 049 (2008) doi:10.1088/1126-6708/2008/01/049 [arXiv:0710.3169 [hep-ph]].
  - [11] J. Kumar, P. Sandick, F. Teng and T. Yamamoto, Phys. Rev. D **94**, no. 1, 015022 (2016) doi:10.1103/PhysRevD.94.015022 [arXiv:1605.03224 [hep-ph]].
  - [12] K. Fukushima, Y. Gao, J. Kumar and D. Marfatia, Phys. Rev. D **86**, 076014 (2012) doi:10.1103/PhysRevD.86.076014 [arXiv:1208.1010 [hep-ph]].
  - [13] L. Bergstrom and P. Ullio, Nucl. Phys. B **504**, 27 (1997) doi:10.1016/S0550-3213(97)00530-0 [hep-ph/9706232].
  - [14] Z. Bern, P. Gondolo and M. Perelstein, Phys. Lett. B **411**, 86 (1997) doi:10.1016/S0370-2693(97)00990-8 [hep-ph/9706538].
  - [15] P. Ullio and L. Bergstrom, Phys. Rev. D **57**, 1962 (1998) doi:10.1103/PhysRevD.57.1962 [hep-ph/9707333].
  - [16] A. Heister *et al.* [ALEPH Collaboration], Phys. Lett. B **544**, 73 (2002) doi:10.1016/S0370-2693(02)02471-1 [hep-ex/0207056].
  - [17] P. Achard *et al.* [L3 Collaboration], Phys. Lett. B **580**, 37 (2004) doi:10.1016/j.physletb.2003.10.010

- [hep-ex/0310007].
- [18] J. Abdallah *et al.* [DELPHI Collaboration], *Eur. Phys. J. C* **31**, 421 (2003) doi:10.1140/epjc/s2003-01355-5 [hep-ex/0311019].
- [19] G. Abbiendi *et al.* [OPAL Collaboration], *Eur. Phys. J. C* **32**, 453 (2004) doi:10.1140/epjc/s2003-01466-y [hep-ex/0309014].
- [20] G. Aad *et al.* [ATLAS Collaboration], *JHEP* **1405**, 071 (2014) doi:10.1007/JHEP05(2014)071 [arXiv:1403.5294 [hep-ex]].
- [21] V. Khachatryan *et al.* [CMS Collaboration], *Eur. Phys. J. C* **74**, no. 9, 3036 (2014) doi:10.1140/epjc/s10052-014-3036-7 [arXiv:1405.7570 [hep-ex]].
- [22] G. Aad *et al.* [ATLAS Collaboration], *JHEP* **1409**, 176 (2014) doi:10.1007/JHEP09(2014)176 [arXiv:1405.7875 [hep-ex]].
- [23] H. Abramowicz *et al.* [ZEUS Collaboration], *Phys. Lett. B* **757**, 468 (2016) doi:10.1016/j.physletb.2016.04.007 [arXiv:1604.01280 [hep-ex]].
- [24] Ya. B. Zeldovich, *Adv. Astron. Astrophys.* **3**, 241 (1965); H.Y. Chiu, *Phys. Rev. Lett.* **17**, 712 (1966); G. Steigman, *Ann. Rev. Nucl. Part. Sci.* **29**, 313 (1979); R.J. Scherrer and M.S. Turner, *Phys. Rev. D* **33**, 1585 (1986).
- [25] C. Kelso, J. Kumar, P. Sandick and P. Stengel, *Phys. Rev. D* **91**, 055028 (2015) doi:10.1103/PhysRevD.91.055028 [arXiv:1411.2634 [hep-ph]].
- [26] M. Ackermann *et al.* [Fermi-LAT Collaboration], *Phys. Rev. D* **91**, no. 12, 122002 (2015) doi:10.1103/PhysRevD.91.122002 [arXiv:1506.00013 [astro-ph.HE]].
- [27] A. Caldwell and M. Wing, *Eur. Phys. J. C* **76**, no. 8, 463 (2016) doi:10.1140/epjc/s10052-016-4316-1 [arXiv:1606.00783 [hep-ex]].
- [28] J. A. Aguilar-Saavedra *et al.* [ECFA/DESY LC Physics Working Group Collaboration], hep-ph/0106315.